

Title: How Honeybees Perceive and Traverse Apertures

Authors: T. Jakobi¹, M. Garratt¹, M. Srinivasan² and S. Ravi¹

Affiliations:

¹ School of Engineering and Information Technology, University of New South Wales Canberra, ACT 2600, Australia

² Queensland Brain Institute, University of Queensland, St. Lucia, QLD 4072, Australia

Abstract

The ability to fly through openings in vegetation allows insects like bees to access otherwise unreachable food sources. The specific visual strategies employed by flying insects during aperture negotiation tasks remain unknown. In this study, we investigated the visual and geometric parameters of apertures that influence honeybee flight. We recorded honeybees flying through apertures with varying shapes and sizes using high-speed cameras to examine their spatial distribution patterns and trajectories during passage. Our results reveal that the flight of bees was, on average, along the bilateral center of the edges of the aperture irrespective of the size. When apertures were smaller, bees tended to also fly closer to the vertical center. However, for larger apertures, they traverse at lower vertical positions (closer to the bottom edge). The behaviors suggest that honeybees modulate their flight trajectories in response to spatial constraints, adjusting trajectory relative to aperture dimensions. When entering at off-center horizontal positions, bees tended to access the vertical center of the aperture, indicating altitude selection influenced by the curvature of the edge below. This behavior suggests an acute awareness of the vertical and horizontal spatial constraints and a preference for maintaining a curvature-dependent altitude that optimizes safe passage. Our analysis reveals that honeybees modulate speed and altitude above the ventral edge passing beneath them, maintaining a median ventral optic flow of 778 deg s^{-1} . This relationship suggests a control mechanism where bees rely on visual information in a narrow ventrally directed field to navigate safely through confined spaces.

Summary Statement: This study reveals how honeybees navigate apertures of varying shapes and sizes, using visual cues and spatial awareness to adjust flight paths for safe and efficient passage.

Introduction

Flying through dense natural environments demands agility and precise coordination, as flyers in these situations must continuously adapt to complex visual and spatial cues to avoid obstacles and find safe passage (Srinivasan, 2011; Serres and Ruffier, 2017). In both natural and urban landscapes, apertures—gaps between foliage or artificial structures—frequently pose navigational challenges, driving the evolution of sensory and motor responses that enable organisms to perform routine foraging, evade predators, and select suitable habitats (Norberg, 2012).

Despite their small size and limited neural resources, flying insects have developed efficient visual processing systems that enable sophisticated navigation in complex environments (Egelhaaf and Kern, 2002). Their compound eyes, which are effectively monocular, provide a wide field of view but offer limited spatial resolution and depth perception (Horridge, 1977). To navigate effectively, bees organize and process optic flow (OF)—the pattern of motion in the visual environment induced by their own movement—from different regions of their eyes: lateral, ventral, dorsal, and frontal, each playing a distinct role in flight control (Gibson, 1950; Srinivasan et al. 1996; Portelli et al. 2011). The ventral region is particularly crucial for maintaining flight speed and altitude, with ventral optic flow playing a key role in speed control, landing, and stabilization (Srinivasan et al., 1991; Izzo and De Croon, 2012; Serres and Ruffier, 2017). Lateral regions assist in horizontal positioning within passages, and bees use lateral landmarks for frontal target acquisition (Lehrer, 1990). The frontal and dorsal regions, with higher visual acuity due to smaller interommatidial angles, facilitate obstacle detection and avoidance (Land, 1997). By segmenting visual input across these specific retinal areas, bees effectively respond to information pertinent to their immediate navigational needs, synthesizing complex spatial information into actionable cues that help regulate flight and navigation through complex environments.

During forward flight, ranging of peripheral objects in the lateral visual field is facilitated by the magnitude of lateral optic flow; closer side objects produce stronger translational optic flow signals, enabling the observer to gauge distance to them (Gibson, 1950; Srinivasan et al., 1996). In the frontal visual field, depth is inferred from the expansional flow that is induced; the rate of expansion is correlated inversely with the distance to frontal stimuli (Srinivasan et al., 1991; Schrater et al., 2001). To optimise unobstructed flight in narrow passages, insects balance the magnitudes of lateral optic flow on both sides, adjusting their trajectory to maintain symmetry and avoid collisions (Tammero and Dickinson, 2002). Consequently, amid confined regions of clutter, flying insects reduce their speed, which constrains the availability of inferable spatial cues (Serres and Ruffier, 2017).

Brightness-based controllers facilitate aperture detection and centering within large-scale regions (Baird and Dacke, 2016). On smaller scales, flying insects enhance navigation and spatial perception through their antennae. Antennae provide airflow mechanosensory signals that enable faster speed estimations compared to relying solely on vision (Fuller et al., 2014). Terrestrial bees have been observed mapping the spatial properties of objects with their antennae (Erber et al., 1997), suggesting that antennal probing aids in perceiving aperture size via tactile feedback. However, the primary technique of pre-traversal aperture evaluation is the execution of rapid reciprocal lateral gazing movements; side-to-side probing of gap edges during flight has been documented (Ravi et al. 2020). This involves comparing the foreground shape to the more distant background, utilizing motion parallax for spatial dimensionalization (Wallace, 1959; Sobel, 1990; Srinivasan et al., 1990; Collett, 2002). When the motion parallax cues are reduced by decreasing the displacement between the foreground and the background, bumblebees execute more vigorous scanning movements (Ravi et al., 2019). These actions facilitate millimeter-accurate postural adjustments for gap traversal (Ravi et al., 2020) and a preference to fly through wider apertures in honeybees during width discrimination tasks (Ong et al., 2017).

In this study, we investigated the speed and position of honeybees as they traversed apertures of varying geometries. Our goal was to determine the visually guided strategies used by the bees to safely traverse through

apertures. By understanding this process, we aim to reveal specialized systems that flying insects use to assess and respond to spatial constraints with greater accuracy.

Materials and methods

Experiment Setup and Procedure

This study was conducted using a colony of honeybees (*Apis mellifera*) housed at the UNSW Canberra campus. Bees were trained to navigate through an indoor tunnel 0.7 m high, 0.4 m wide, and 1.16 m long (Fig. 1A). It was constructed from a 5 mm thick twin-wall extruded corrugated plastic sheet material (also known by its trade name Corflute). The experimental setup featured an entrance aperture at one end of the tunnel measuring 5 cm in diameter and an outlet aperture measuring 6.5 cm in diameter. At the far end of the interior of the tunnel (directly below the outlet), a chamber was equipped with a gravity feeder dispensing a homemade 10% sucrose solution (Fig.1). To facilitate orientation and visual processing, the walls and floor of the tunnel were lined with a black and white 1/f noise cloud pattern offering a mean contrast of 50%, which is consistent with visual stimuli used in related studies (Ravi et al., 2019; Monteagudo et al., 2022). To mitigate potential behavioural influences on the bees caused by contrast changes in the 1/f pattern, we applied a checkered texture to the area on the wall (perpendicular to the tunnel walls) surrounding the apertures (Fig. 1B). This texture was designed to provide consistent visual stimuli, reducing the likelihood of unintended visual cues affecting the bees' navigation behaviour while still providing visual texture for motion awareness. The ceiling of the tunnel was made from a transparent UV-blocking acrylic sheet, allowing natural lighting from above.

Foraging bees were trained to fly through the tunnel by placing a cotton bud soaked in sugar solution at various incremental positions along the tunnel. This approach enabled the bees to learn the location of the food source and resulted in a consistent cycle of keen bees travelling one way through the tunnel. After this initial training, the bees consistently returned to the tunnel without further conditioning. After several days of habituation, we introduced a wall midway through the tunnel which presented an aperture of varying diameters and shapes (Fig. 1A-B). After inserting the wall, the setup required bees to negotiate the aperture in the wall to access the food source. The feeder was positioned at the far end of the tunnel section on the other side of the wall. It sat on a symmetrical platform raised 28 cm above the floor with the base of the feeder (bright yellow) aligned with the midline ($y = 0$) of the tunnel (Fig. 1A). The center of each interchangeable aperture was aligned with this height along the longitudinal axis of the tunnel, ensuring that the centroid of each aperture corresponded to the $Y = 0, Z = 0$ (X -axis) intersection of the wall plane within the tunnel. This alignment ensured a straight line of sight from the tunnel inlet, through the aperture, and to the feeder at the opposite end, regardless of the aperture's size or shape (Fig. 1B). The camera was just below this axis of alignment, making the flight path of bees visible from aperture approach to landing on the feeder.

Bees were given three hours to acclimate to newly interchanged apertures on the wall in the tunnel setup. This was done on separate days before commencing bee recordings. Experiments were conducted sequentially, with a new aperture introduced in the morning, followed by the acclimation period for the bees before recording began. Bees were not individually tagged, which is a limitation of this study as it prevents the identification of individual bees. However, the high frequency of forager activity (20 flights per minute) and the irregular nature

of each test session (random days over a two-month period during summer) was considered sufficient to eliminate data biasing through repeated trials by individuals, ensuring that the recorded data reflected initial navigational responses to the aperture challenge.

After a manual assessment of the recordings, only flights through the apertures that were direct, without hesitation, and free from interference by other bees in the tunnel were included as data samples. We observed a marked difference between the flights of untrained (or "new") bees and those of trained bees. Trained bees consistently made direct flights to the food source on the opposite side of the wall. It was evident that bees learned to access the food source more rapidly with larger apertures, likely due to the wider and more accessible openings. To maintain consistency in tests, the same training duration was used for all aperture changeovers. Each experimental session lasted one hour during peak foraging times, providing at least 500 recorded bee movements through each of the 11 aperture types tested.

Data Acquisition

We positioned a GoPro 11 camera just beneath the tunnel inlet, approximately 30 cm above the ground, such that the centre of the lens aligned with the vertical plane going through the longitudinal axis of the tunnel (Fig. 1A). The camera view was just below the longitudinal X axis running through the centre of the apertures and feeder, facing the obstacle wall, to provide an orthogonal perspective of that plane (Fig. 1B). This setup ensured that the location of the bees' entries on the wall plane (YZ) could be accurately captured. Additionally, a thin mirror, sized 4 cm x 15 cm was used to provide an overhead (XY) view of the bees as they navigated through the apertures. This mirror was adjusted to a 43-degree slant angle (from horizontal) so that a top-down view of the aperture was possible from the camera positioned just below the X-axis of the tunnel (Fig. 1). A 3D coordinate system with its origin in the centre of the apertures was constructed using the frontal view for YZ coordinates and the top-down view for XY coordinates, as shown in Fig. 2A. With this setup, the camera captured the point where the bees intersected the plane of the wall (and aperture), and the entry time, which was used in the front-facing view for determining the entry position of the bees.

Videos were captured at a frame rate of 120 fps. Post-processing was conducted using custom MATLAB code, which involved manual image-based coordinate digitization. Spatial calibration (converting pixels to metric units) was achieved by using the known aperture dimensions in the two different views (XY and YZ) of the aperture (frontal and mirror views). To verify the X-axis calibration and the location of intersection with the wall plane, snapshots of a handheld measuring scale directed along the X-axis at the centre of the apertures were analysed to accurately mark the intersection point of the YZ plane (relative to the XY view) in the downward-facing mirror view.

Entry locations and times for each bee at the apertures were identified by manually scrolling through video frames, using both the top-down mirror view (XY plane) and the axially directed frontal view (YZ plane). In addition to digitally marking the XY entry locations, the presence of any form of collision (from the wing, body, or legs on the perimeter of the aperture) was noted, marked and categorised. In 50 entry samples for each of the apertures, the position of the distal tip of the abdomen was digitized in two consecutive frames to estimate the speed at the time of entry (Fig. 2B).

Motion Perception Analysis

The analysis of our experiments involved calculating optic flow as bees flew through circular and elongated circular apertures. Taking the case of the isotropic circular aperture as an example, we utilized formulae based on the visual angle θ subtended by the edges of the aperture between two reference time steps (t_1 and t_2) (Fig. 2C), calculated as:

$$\theta = 2 \cdot \tan^{-1}\left(\frac{r_d}{\Delta x}\right) \quad (1)$$

where r_d is the distance to the nearest edge of the aperture, given by $r = \sqrt{y^2 + z^2}$, and Δx is the distance along the longitudinal (X) axis between the two time-referenced points (t_1 and t_2) to the plane of the aperture (YZ).

The rate of change of this subtended angle (θ), with respect to time, provides a measure of optic flow (Ω) in radians per second ($rad\ s^{-1}$):

$$\Omega = \frac{d\theta}{dt} = \frac{d}{dt}\left(2 \cdot \tan^{-1}\left(\frac{r_d}{x}\right)\right) \quad (2)$$

These equations represent the total optic flow experienced by the bee as it moves through the aperture, capturing how the entire visual scene expands or contracts in the bee's field of view as it approaches or passes through. However, while informative, these calculations may obscure the relationships with specific edges in scenarios where interactions with single edges may be more relevant—such as when bees navigate close to structural features. To refine our approach, we calculated the optic flow generated by the movement over particular edges, casting rays to each edge of interest (see the ventral edge example displayed in Fig. 2C).

For these ray-edge interactions, we adopted a simplified optic flow ($rad\ s^{-1}$) formula:

$$\Omega = v/r_d \quad (3)$$

where v is the axial velocity (along X) of the observer during traversal, and r is the ray distance to the edge of interest (at t_2). The approximation assumes linear and perpendicular motion of the observer relative to the edge, reducing the complexity at the critical moment of sensory input during traversal. The formula is derived using the small-angle approximation ($\tan(\theta) \approx \theta$ when θ is small), which simplifies the relationship between optic flow and angular motion. While this simplified approach has limited applicability to complex, realistic environments, it effectively captures the fundamental optic flow relationship and enables focused analysis of specific regions within the aperture.

$$\Omega_{BL} = \frac{\left(\frac{v}{r_{d\text{left}}}\right) + \left(\frac{v}{r_{d\text{right}}}\right)}{2} \quad (4)$$

$$\Omega_{DV} = \frac{\left(\frac{v}{r_{d\text{dorsal}}}\right) + \left(\frac{v}{r_{d\text{ventral}}}\right)}{2} \quad (5)$$

$$\Omega_R = \frac{1}{360} \sum_{i=1}^{360} \frac{v}{r_{d_i}} \quad (6)$$

$$\Omega_V = \frac{v}{r_{\text{ventral}}} \quad (7)$$

To examine how different regions of apertures influence the bee's optic flow during traversal, we used an assortment of optic flow quantification approaches tailored to prominent edges within specific areas of the visual field, all measured in radians per second (see Eqn 4–7). These include: bilateral optic flow (Ω_{BL}), which sums the motion from the left and right edges (Eqn 4); dorsoventral optic flow (Ω_{DV}), which sums the motion from the top and bottom edges (Eqn 5); radial optic flow (Ω_R), which is the average edge motion calculated by casting rays in 360 directions around the aperture (Eqn 6); and ventral optic flow (Ω_V), which captures the motion from the edge directly beneath the bee (Eqn 7). The unidirectional (Ω_V) and bi-directional optic flows (Ω_{BL} , Ω_{DV}) use rays cast horizontally or vertically from the entry point of the bee to the nearest edge as illustrated in Fig. 4B.

Statistics and Data Interpretation

Statistical analyses were performed on the bees' entry location data across apertures of varying sizes, with sample sizes ranging from 100 entries for the smallest aperture to over 500 entries for the larger apertures. The variation in sample sizes was partly attributable to differences in traversal success rates and the necessity to accurately sample the broader spatial distribution inherent in larger apertures. A sample size of 100 entries was deemed sufficient to achieve comprehensive data coverage across each of the spanwise bins for the smallest aperture, ensuring that each bin was adequately represented relative to its absolute area. In contrast, larger apertures required increased sample sizes to effectively capture the expanded spatial distribution within each bin, thereby maintaining representative coverage across the larger aperture space.

To facilitate consistent and representative analysis of velocity and optic flow, a stratified random sampling approach was employed. The aperture plane was divided into three equi-spaced spanwise bins on each semi-circular half of the apertures. From each bin, velocity analysis was performed on 10 random samples. These samples were chosen from either semi-circular side, resulting in a total of 30 samples (with varying lateral positions) for each optic flow group per aperture before data filters were applied (see Table 1 for sample sizes post-filter for each set). This sampling method minimized central sampling bias by evenly distributing pre-filter dataset sizes across the spanwise bins, ensuring coverage of the entire aperture width.

Throughout this report data are expressed in the form *Median* \pm *MAD* to minimise the influence of skewness and outliers. In our visual representations of the raw entry data (Fig. 3), standard deviations are used to collate the raw positional data, facilitating straightforward interpretation and comparison with prior studies that have traditionally employed mean-based metrics.

For OF data, percentile thresholds at the 5th and 95th percentiles were used to exclude the top and bottom 5%, eliminating outliers from measurement errors or atypical behaviors unrepresentative of the general foraging population. Comparing OF variability within and between the datasets was conducted using median-based statistical metrics including the Interquartile Range (IQR), Median Absolute Deviation (MAD) (calculated without scaling), and Coefficient of Variation of the Median (CV_{Med}) as shown in Table 1. These metrics are less sensitive to outliers (than mean-based counterparts) and provide a reliable measure of dispersion around the median, making them suitable for skewed data distributions common in behavioral studies. These were considered robust measures of variability in the non-normally distributed data to complement statistical analyses and were used to infer the underlying controllers that the subjects of these experiments might be using.

To assess the statistical significance of differences in optic flow datasets across various aperture sizes and shapes, we employed non-parametric hypothesis testing due to the violations of normality assumptions in the datasets. For pairwise comparisons between two independent groups, we used the Mann-Whitney (MW) U tests. For comparisons involving three or more groups, we used the Kruskal-Wallis (KW) H test to determine whether there were statistically significant differences in the median ranks of independent groups. After obtaining a significant KW test result ($p < 0.05$), we conducted post-hoc pairwise comparisons using Dunn's test with Bonferroni corrections to identify which specific groups differed from each other. We also computed effect sizes to quantify the magnitude of differences. For multi-group comparisons using the KW test, we calculated epsilon-squared (ϵ^2) as a measure of overall effect size for the KW test using $\epsilon^2 = \frac{H - (k - 1)}{N - k}$, where H is the KW test statistic, k is the number of groups, and N the total sample size. For pairwise comparisons, we derived a standardized effect size as $r = \frac{Z}{\sqrt{N}}$, where Z is the (signed) z-score corresponding to the MW test result. We reported sample sizes (n), test statistics (H for KW tests, U for MW tests), p -values, and effect sizes (r and ϵ^2) were reported in the results (see Tables S4-6).

Results

Bees' flight behaviours in the tunnel

We manually digitized entry and collision locations of bees to analyse the distributions of aperture traversal locations. Observations of individual flights revealed that bees generally flew directly through the tunnel, maintaining their trajectory towards the feeder while performing some lateral oscillations (also known as casting). Before traversing the aperture wall, bees typically aligned themselves with the gap as a preparatory adjustment for imminent passage. Occasionally, bees approached at non-orthogonal angles—typically near the sides—and exhibited increased lateral motion.

Following the initial approach, bees traversed the apertures at varying axial speeds and positions in the YZ plane. After passing through an aperture, bees continued directly to the feeder platform on the opposite side of the wall. Immediately after passing through the aperture, bees exhibited a sudden drop in altitude, which was more pronounced when flying through smaller-diameter apertures. Subsequently, there was a noticeable ascent as the bees reached the feeder.

Bees that were unsuccessful in avoiding collision while passing through the aperture typically displayed a poorly controlled trajectory within the aperture space. For bees experiencing wing collisions, we observed an

immediate roll toward the side of the collision and a sudden drop in altitude. This was followed by an overcorrection, causing a rapid lateral displacement as the bee passed through. Subsequent oscillations in roll orientation and loss of lateral control were observed during the remainder of the traversal through the aperture and the subsequent path to the food source. Body collisions typically occurred when bees used lateral manoeuvring to sideslip through when close to the edges on one side of the opening. Leg collisions were less pronounced and were usually observed as the legs being dragged harmlessly over the bottom edge of the aperture, rather than being associated with any significant impact.

Entry and Collision Locations Across All Apertures

Tests were divided into three categories (Fig. 3 and Table 1): (A–E) circular apertures with varying diameters (30 mm to 150 mm), (F–G) mid-sized apertures (60 mm diameter) with extended lateral or vertical sides (created by adding straight-edged sections between two semi-circular halves), and (H–K) mid-sized circular apertures (60 mm diameter) with varying surrounding visual textures. For each aperture type, we digitized the vertical (Z-axis) and lateral (Y-axis) entry coordinates of at least 100 bee flights, as shown in Fig. 3, providing a detailed view of the distribution of bee entry positions across aperture geometry types.

Across all aperture types, the median lateral entry position was centered between the left and right edges (Table 1, Fig. 3), indicating that bees tended to enter at the bilateral midpoint of the aperture. In contrast, the vertical entry position (Z-axis) showed a consistent tendency for bees to pass through the lower half of the aperture—a trend that became more pronounced with larger apertures. For the smallest aperture (A, $D = 30$ mm), most bees entered near the center of the aperture (median lateral position ($Y = 0.21$ mm), median vertical position ($Z = 0.24$ mm)), as indicated by the blue median marker in Fig. 3A. In the largest aperture (E, $D = 150$ mm), the median vertical entry position was significantly below the center ($Z = -24.9$ mm), while the median lateral position remained approximately centered ($Y = 1.06$ mm).

Smaller apertures exhibited lower positional variation as shown by the standard deviations (and mean absolute deviations) in both lateral and vertical entry positions (see green boxes in Fig. 3). For the smallest aperture, the standard deviations were $\sigma_Y = 6.56$ mm (lateral) and $\sigma_Z = 5.51$ mm (vertical). These values increased approximately linearly with aperture size, reaching $\sigma_Y = 22.44$ mm and $\sigma_Z = 29.28$ mm for the largest aperture (Fig. 3). This trend persisted even when standard deviations were normalized by the aperture radius (Table 1 and Table S11).

Collisions with the edges of the circular apertures were more frequent in smaller apertures compared to larger ones (Fig. 3A–E and Table 1). In the smallest aperture (A, diameter 30 mm), 61.5% of the bees experienced collisions, whereas only 10.3% did so in the largest aperture (E, diameter 150 mm). In aperture A, most collisions (96.7%) involved the bees' wings, with less than 10% involving body collisions upon entry or during traversal (Table 1). Bees that made wing contact with the aperture edges experienced significant roll perturbations, adversely affecting their flight stability and often resulting in downward veering to one side. Bees that made edge contact involving their bodies (abdomen, thorax, or legs) were less impacted in their subsequent flight behavior.

In general, smaller circular apertures showed a higher proportion of wing collisions compared to body collisions (Fig. 3A-E and Table 1). In larger apertures, most of the fewer observed collisions were body strikes, comprising 82.3% of collisions in aperture E. Wing collisions generally occurred in the upper half of the apertures, while body collisions were more common in the lower half (Fig. 3). It was common to observe bees with body strikes 'brushing' their legs against the bottom edge of the aperture. Although these instances were recorded as collisions, they had minimal influence on the bees' flight trajectories.

The traversal velocity of bees increased with the diameter of the circular apertures (Fig. 4A). In the largest aperture (E, 150 mm), bees' median flight traversal speeds ($v_x = 0.57 \pm 0.15 \text{ m s}^{-1}$) approached the speeds in the tunnel without any aperture wall obstruction ($v_x = 0.76 \pm 0.15 \text{ m s}^{-1}$). The total optic flow produced by the edges of the apertures generally increased with aperture diameter, peaking for apertures between 60 mm and 90 mm diameter and then decreasing for larger apertures across Ω_{BL} , Ω_{DV} , and Ω_R OF measurements. For Ω_V , the median optic flow magnitudes ranged narrowly about the median of $778 \pm 31 \text{ deg s}^{-1}$ (IQR = 66 deg s^{-1} , range = 137 deg s^{-1}), as shown in Fig. 4B iv., exhibiting less absolute variation than in the other OF measurements (Table 2, S4 and S6).

Flights through the horizontally and vertically elongated apertures (Fig. 3F-G) demonstrated the influence of aperture shape on bee entry locations. These apertures were created by retaining the curvature of the 60 mm circular aperture while extending only the width (horizontal elongation, aperture F) or the height (vertical elongation, aperture G). In the horizontally elongated aperture, bees traversed at a position closer to the lower edge relative to the aperture height (median vertical position $Z = -9.88 \pm 10.46 \text{ mm}$), whereas in the vertically elongated aperture, bees traversed relatively closer to the center ($Z = -12.31 \pm 23.41 \text{ mm}$). In both cases, bees maintained horizontal centering (median lateral positions $Y = 2.21 \pm 15.36 \text{ mm}$ and $Y = -0.04 \pm 14.17 \text{ mm}$, respectively). The mean absolute deviation was greater in the direction of elongation for each aperture, and relatively greater for the vertically elongated shape ($MAD_Y = 15.36 \text{ mm}$, $MAD_Z = 10.46$ for aperture F, and $MAD_Y = 14.17$, $MAD_Z = 23.41$ for aperture G).

Only 10% of bees exhibited edge collisions during traversal of the horizontally elongated aperture (F), approximately three times less than the 60 mm circular aperture (28%, Table 1). More than 50% of bees experienced collisions in the vertically elongated aperture (Fig. 3 and Table 1 F-G), which was more than double the rate of collisions in the 60 mm circular aperture. Of these, 67% were body/leg collisions in the horizontal aperture, with more than half brushing their legs or touching the lower edge. In the vertical aperture, 94% of all collisions were wing collisions, comparable to the ratio for the 60 mm circular aperture (Table 1). Body collisions in both elongated shapes tended to occur at the lower sections of the aperture rim similar to all other tested apertures as shown in Fig. 3F-G.

Velocities through the horizontally and vertically elongated apertures (F-G, Fig. 5A and Table S2) were not statistically different than those through the circular aperture of the same minor axis diameter (Aperture B, 60 mm diameter) (Fig. 5A and Tables S1, S14 and S15). The speeds and bilateral and dorsoventral optic flow measurements compared between apertures F and G were significant (Fig. 5 Bi-iv, Tables 3 and S2), suggesting strong influence of aspect ratio on the traversal strategies of bees.

In the horizontally elongated aperture, bees' entry locations were proportioned similar (both close to the $-1/3$ normalised height) to those in the circular aperture of the same lateral scale (120 mm, Aperture D) as shown in Fig. 3F and Fig. 3D. However, due to aspect ratio differences, absolute heights were reduced compared to both the 60 mm and 120 mm circular apertures (Fig. 3F and Table 1). Being closer to the edge below, they traversed at significantly slower speeds than the 120 mm aperture (corresponding to the major axis in width) and similar speeds as the 60 mm aperture (corresponding to the minor axis in height of the horizontally elongated aperture). In the vertically elongated aperture, bees also flew at entry locations proportional to the 120 mm aperture (in height) but at significantly lower speeds slower that were comparable to both the 60 mm and horizontally elongated apertures (Fig. 5A). However, they flew at absolute heights significantly greater than both the 60 mm and 120 mm diameter circular apertures. This resulted in significantly lower ventral optic flow compared to all other apertures (Fig. 5B).

To investigate the role of surrounding textures on traversal, we examined the effect of removing visual textures surrounding specific halves of the 60 mm circular aperture—lower, upper, right, or left (Fig. 4B, H-K). The distributions of entry locations were biased towards the texture-flanked half as shown in Table 3. The bias was significant when comparing the group bilateral entry distributions for left and right texture-flanked halves with the 60 mm plain texture aperture, as indicated by the significant p-value yielded from the omnibus test of three groups ($p = 0.0053$) (Table S8). Subsequent pairwise tests between the three groups revealed a significant comparison only between the left flanked and the right flanked datasets ($p = 0.0036$), but not against the uniform control (Tables 3, S8, and S10). Biases were insignificant when group-comparing the horizontal and vertical coordinate datasets of upper and lower texture-flanked halves and the uniform control ($p = 0.7502$ for Y, $p = 0.1030$ for Z coordinates) (Table S8). Although the overall group comparisons test did not yield significance (Table S5), Dunn's post-hoc pairwise tests were performed for all pairs to maintain consistency with the comparison of side-flanked set where a significant test result was observed (see Table 3 and S10). The pairwise comparison test yielded a p-value of 0.1004 for the Z coordinates between the two vertically flanked tests (H and I) (Tables 3 and S9), which approaches the significance level but does not meet the criteria for confirming the trend.

Bees displayed similar speeds when flying through the reduced-texture 60 mm apertures (Fig. 6A, H-K), with a median velocity of $v_x = 0.31 \pm 0.13 \text{ m s}^{-1}$, compared to the fully textured 60 mm aperture ($v_x = 0.30 \pm 0.09 \text{ m s}^{-1}$) (Tables S1 Table S3). The non-parametric group comparison test (KW) returned a non-significant p-value ($p = 0.8885$) (Table 4), indicating no significant difference in traversal speed between the different aperture conditions. The optic flow measurements across all apertures showed similar relative variabilities and were not significantly different when compared among each other.

Collisions for each texture-flank location and aperture edge are shown in Table S7. An omnibus Chi-Square Test for Homogeneity indicated no overall difference in distribution of collisions across edges among the five edges when flanked with different locations of texture ($\chi^2 = 11.95$, $df = 12$, $p = 0.449$). To probe potential differences between individual edges, we performed separate 2×4 chi-square tests (unadjusted). Only the comparison between "Left Flanked" and "Right Flanked" reached nominal significance ($p = 0.047$), but this difference does not remain significant after a Bonferroni multiple-comparison correction. We therefore conclude

that there is no statistically meaningful difference between any pair of collision-texture location conditions once we control the familywise error rate.

Discussion

Centralized Traversal of Narrow Apertures

Our study investigated how bees navigate through apertures of varying sizes and shapes, challenging the hypothesis that they would consistently fly through the center—a path theoretically offering maximal clearance and minimal collision risk. When navigating through small apertures (30–60 mm diameter), bees exhibited geometric centering behavior both laterally and vertically, minimizing the risk of collision with the edges (Fig. 3). This centering behavior is consistent with the idea that bees rely on the balance of symmetrical visual cues from the surrounding edges to guide their flight in confined spaces (Srinivasan et al., 1996; Srinivasan and Zhang, 1997). The proximity of both lateral and vertical boundaries provides strong bi-directional optic flow cues that enable bees to maintain a centered trajectory.

Analysis of lateral positions across all aperture diameters showed that the absolute standard deviations of bee entry positions increased proportionally with the widths of the apertures (Table 1). However, relatively, lateral entry positions of bees were consistently confined within the central one-third band of the apertures, regardless of diameter (Fig. 3 and Table S12). This pattern was maintained in the elongated apertures, indicating that bees regulate their lateral positioning relative to the proportions of the aperture. Tighter absolute spatial constraints in smaller apertures demand flight precision within the narrower absolute dimension of the band. By maintaining a proportional distance within the physical boundaries of the aperture, bees seem to optimize their movement for safest passage with respect to their wingspan.

As the aperture size increased, bees displayed less vertical centering behavior, opting instead to fly closer to the lower edge of the aperture. This shift suggests that in larger apertures, where spatial constraints are reduced and the risk of collision is lower, bees do not prioritize centering; instead, they adopt alternative strategies, possibly relying more on ground-based visual cues. The decreased vertical centering in larger apertures and the tendency toward the lower edge imply that bees are using a flight strategy based on a preferred fixed edge—the bottom edge. In large spaces, where the consistency in relative standard deviation (vertical lines of the green boxes in Fig. 3) represents a greater absolute dimension, the need for precise centering diminishes.

The transition from centering behavior in small apertures to favoring flight near the lower rim in larger apertures may reflect an inherent trade-off between the benefits of centering and the costs associated with maintaining it. Precise centering requires continuous processing of visual cues from both bilateral and dorsoventral fields and frequent course corrections, which may be energetically costly. In larger apertures, the reduced necessity for such lateral precision allows bees to simplify their flight control and conserve energy for other complex behavioral demands.

Adaptive Traversal Altitude

Building upon our observations that bees center their flight relative to aperture edge curvature, we investigated the influence of the ventral edge on entry height distributions. We grouped data from pairs of bins equidistant from the center—Outer (bins 1 and 6), Middle (bins 2 and 5), and Inner (bins 3 and 4)—to represent regions of varying curvature along the ventral edge, forming vertical trisectors (Fig. 7A, B).

After normalizing entry heights by aperture radius (R), we found that in the outer trisector—where vertical space is most constrained ($1.1 R$, Table S12)—bees consistently maintained an entry height of approximately 0.5 - $0.6 R$ above the ventral edge across all aperture sizes (Figure 7B, Table S12). The bees aligned near the vertical center of the available space when traversing the outer third of circular apertures (Fig. 7), consistent with the vertical centering behavior observed in small diameter-constrained apertures (Fig. 3). In the inner bins near the aperture center—where vertical space is less constrained—the bees' normalized entry heights varied more with aperture size (Fig. 7B and Table S12). In the smallest apertures, bees in the innermost bins exhibited higher median normalized heights of around $1R$ above the ventral edge (Fig. 7B and Table S12), effectively maximizing clearance (Table 6).

The bees' tendency to maintain this relative height when free of spatial pressures suggests reliance on a simple proportional metric—like our division into proportional sectors—as a simple strategy for safe traversal, requiring minimal computational effort by leveraging the aperture's relative geometry during flight. By maintaining an entry height of 0.5 - $0.6 R$ when space is imposing in a particular vertical segment, collision avoidance is optimised in varying aperture geometries, particularly within the outer trisector.

Ventral Optic Flow Controller in a Narrow Visual Field

Speed is proportional to the aperture entry location relative to the edges, as bees fly slower near surfaces which produce large OF signals (Srinivasan et al., 1996). Incorporating speed into our analysis of flight altitude reveals that the observed vertical distances to the edge below are correlated to ventral OF, with bees maintaining ventral edge distances that on average correspond with their flight speed, thereby keeping ventral OF in a consistent range (see Fig. 8). In larger apertures, bees entering near the sides—where the vertical distance to the edge below is lower due to rim curvature—maintained velocities comparable to central regions (no significant differences between trisectors in Fig. 8A) by raising their flight altitude. This altitude adjustment allows them to preserve consistent ventral OF without significant changes in speed (Fig. 8B). However, in smaller apertures, the limited space between the dorsal and ventral edges restricts altitude adjustments, creating a dilemma that leaves centering as the only viable option. As a result, bees are forced to reduce their speed near the edges to keep ventral OF consistent.

One prevailing hypothesis is that bees process optic flow across their entire visual field to detect discontinuities and locate the center of an aperture. However, this strategy might be complex and error-prone due to the difficulty of integrating extensive visual information. An alternative, simplified flight control strategy that focuses on stabilizing ventral OF—which is key data in other modes of flight—could be more effective. This

approach would enable bees to navigate safely through narrow, elevated passages by intuitively measuring their speed and distance relative to proximal edges beneath the observer.

Across circular apertures of all sizes and at all lateral locations of entry, bees maintain a ventral OF with a relatively confined range of 778 deg s^{-1} (IQR = 66, range = 137) (Fig. 8B). In larger apertures, flying near the side edges reduces the vertical distance to the ventral edge, causing a surge in the perceived passing rate of edges in the scene beneath, thereby increasing ventral OF. In response, the ventral OF controller adjusts elevation accordingly to optimise clearance. In smaller apertures, where dorsoventral balancing pressure may oppose altitude increases, ventral optic flow can be sustained by reducing velocity.

Ventral Optic Flow Controller in Elongated Apertures

We evaluated the effectiveness of the proposed ventral OF controller in elongated apertures (apertures F and G). If bees utilize a simple OF controller based on their height above the lower edge and speed adjustments, we would expect similar behavioral patterns relative to the OF generated by the lower edge in both circular and non-circular apertures. However, our observations revealed deviations from this expectation (see Fig. 5). In horizontally elongated apertures, bees flew at lower altitudes and maintained similar speeds compared to the 60 mm circular aperture. In vertically elongated apertures, bees flew at higher altitudes above the bottom edges and at slower speeds compared to other relevant apertures, resulting in a significantly lower ventral OF.

These findings indicate that an aperture's aspect ratio influences the relative weighting of OF cues for speed regulation and positioning. The results imply that bees exhibit a behavioral response to the shape of non-circular apertures, potentially perceiving their spatial layout in relation to their own body dimensions and adjusting their flight paths accordingly to minimize collisions, as observed in other gap challenge examples in the literature (Ravi et al., 2020). In narrow vertical apertures, reduced horizontal width increases lateral OF from closer side edges. This likely prompts bees to maintain a more central position, potentially compensating for the weaker ventral OF caused by the more distant lower edge. This behavior suggests that bees rely more heavily on lateral OF cues when they are more prominent, similar to how they regulate speed when flying through narrow corridors with close side walls (Srinivasan et al., 1996; Baird et al., 2010).

Influence of Visual Texture on Aperture Passing Strategies.

The preferential entry toward texture-flanked sides seen in the results suggests that bees utilize visual textures as key cues for aperture traversal. They favour areas with richer visual information, tending to enter closer to those sides, with a stronger preference towards laterally arranged textures compared to vertically arranged ones. Anatomically, bees' have higher resolution in the frontal regions due to the ommatidia arrangement in their compound eyes, which augments their sensitivity to lateral and ventral cues (Hecht and Wolf, 1929; Seidl and Kaiser, 1981). Additionally, their flight dynamics—characterized by lateral motion inertial sensitivities and

thrust vectoring for control (Ravi et al., 2013; Crall et al., 2015)—facilitate rapid horizontal repositioning during traversal, which could explain why there was stronger bias toward lateral textures.

Despite the biases, traversal speeds remained consistent across all aperture texture conditions (Fig. 6A, $p = 0.8885$, Table 4), indicating that reduced surrounding texture has little influence on traversal OF cues. Similarly, the absence of significant differences in optic flow measurements across texture conditions (Fig. 6Bi-iv) supports the notion that bees primarily rely on the detection of edges—rather than the surrounding surface texture—for shape discrimination and navigation. This aligns with previous literature indicating that bees use contrast and brightness gradients in their photoreceptor channels, making untextured edges less discernible than textured ones (Lehrer et al., 1990; Horridge, 2015; Srinivasan and Lehrer, 1988). The contrasting may allow them to perceive aperture boundaries upstream, gleaning geometric data on the obstacle before reaching the target challenge. The bias toward textured sides may be due to the enhanced contrast and visual salience provided by textures in particular regions during approach, facilitating preparatory localisation before transit.

Thus, while richer visual textures may enhance the visual salience of certain sides of the aperture, facilitating earlier and more confident localization, the fundamental cue for controlled passage appears to be the presence and orientation of edges. Once edges are detected, bees likely rely on OF generated by these boundaries—especially the ventral edge—to guide their movement. This combination of textural preference during approach and edge-based navigation during the fine control needs of traversal underscores a sophisticated and adaptive visual guidance strategy in bees.

Implications for Insect Navigation

Apertures are ubiquitous in both natural and urban environments, making the ability to efficiently perceive and navigate through them indispensable for flyers like bees and other insects. Our findings indicate that bees may integrate visual information in a manner that prioritizes certain optic flow cues, particularly the ventral edge of an aperture, during traversal. Our data cannot definitively confirm the existence of a dedicated ventral optic flow controller, but it shows how bees selectively utilize specific regions of their visual field when navigating constricted spaces adapting their trajectories to manifest this. This observation aligns with theories linking localized visual processing tactics to specific flight tasks (see Lecoœur et al., 2019), reinforcing that monocular vision-based flyers do not need to process optic flow across their entire field of view. These insights deepen our understanding of insect navigation strategies and can serve as inspiration for designing bio-inspired, resource-efficient algorithms for robotic navigation in complex environments.

Acknowledgements

This research was partially supported by the Australian Government through the Australian Research Council's Discovery Projects funding scheme (project DP220101883) and by the Asian Office of Aerospace Research and Development (AOARD) (Grant No. FA2386-21-1-4075 and FA2386-23-1-4033).

References

- Baird E, Dacke M (2016) Finding the gap: a brightness-based strategy for guidance in cluttered environments. *Proceedings of the Royal Society B: Biological Sciences* 283:20152988
- Collett TS (2002) Insect vision: controlling actions through optic flow. *Current Biology* 12:R615–R617
- Crall JD, Ravi S, Mountcastle AM, Combes SA (2015) Bumblebee flight performance in cluttered environments: effects of obstacle orientation, body size and acceleration. *J Exp Biol* 218:2728–2737
- Egelhaaf M, Kern R (2002) Vision in flying insects. *Curr Opin Neurobiol* 12:699–706
- Erber J, Pribbenow B, Grandy K, Kierzek S (1997) Tactile motor learning in the antennal system of the honeybee (*Apis mellifera* L.). *Journal of Comparative Physiology A* 181:355–365
- Fuller SB, Straw AD, Peek MY, et al (2014) Flying *Drosophila* stabilize their vision-based velocity controller by sensing wind with their antennae. *Proceedings of the National Academy of Sciences* 111:E1182–E1191
- Gibson JJ (1950) *The perception of the visual world*.
- Hecht S, Wolf E (1929) The visual acuity of the honey bee. *J Gen Physiol* 12:727–760
- Horridge GA (1977) The compound eye of insects. *Sci Am* 237:108–121
- Izzo D, De Croon G (2012) Landing with time-to-contact and ventral optic flow estimates. *Journal of Guidance, Control, and Dynamics* 35:1362–1367
- Land MF (1997) Visual acuity in insects. *Annu Rev Entomol* 42:147–177
- Lecoeur J, Dacke M, Floreano D, Baird E (2019) The role of optic flow pooling in insect flight control in cluttered environments. *Sci Rep* 9:7707
- Lehrer M (1990) How bees use peripheral eye regions to localize a frontally positioned target.
- Monteagudo J, Egelhaaf M, Lindemann JP (2022) Random attention can explain apparent object choice behavior in free-walking blowflies. *Journal of Experimental Biology* 225:jeb243801

- Norberg UM (2012) Vertebrate flight: mechanics, physiology, morphology, ecology and evolution. Springer Science & Business Media
- Ong M, Bulmer M, Groening J, Srinivasan M V (2017) Obstacle traversal and route choice in flying honeybees: Evidence for individual handedness. *PLoS One* 12:e0184343
- Portelli G, Ruffier F, Roubieu FL, Franceschini N (2011) Honeybees' speed depends on dorsal as well as lateral, ventral and frontal optic flows. *PLoS One* 6:e19486
- Ravi S, Bertrand O, Siesenop T, et al (2019) Gap perception in bumblebees. *Journal of Experimental Biology* 222:jeb184135
- Ravi S, Crall JD, Fisher A, Combes SA (2013) Rolling with the flow: bumblebees flying in unsteady wakes. *Journal of Experimental Biology* 216:4299–4309
- Ravi S, Siesenop T, Bertrand O, et al (2020) Bumblebees perceive the spatial layout of their environment in relation to their body size and form to minimize inflight collisions. *Proceedings of the National Academy of Sciences* 117:31494–31499
- Schrater PR, Knill DC, Simoncelli EP (2001) Perceiving visual expansion without optic flow. *Nature* 410:816–819
- Seidl R, Kaiser W (1981) Visual field size, binocular domain and the ommatidial array of the compound eyes in worker honey bees. *J Comp Physiol* 143:17–26
- Serres JR, Ruffier F (2017) Optic flow-based collision-free strategies: From insects to robots. *Arthropod Struct Dev* 46:703–717
- Sobel EC (1990) The locust's use of motion parallax to measure distance. *J Comp Physiol A* 167:579–588
- Srinivasan MV, Lehrer M, Horridge GA (1990) Visual figure–ground discrimination in the honeybee: the role of motion parallax at boundaries. *Proceedings of the Royal Society of London B Biological Sciences* 238:331–350
- Srinivasan M V (2011) Visual control of navigation in insects and its relevance for robotics. *Curr Opin Neurobiol* 21:535–543
- Srinivasan M V, Lehrer M, Kirchner WH, Zhang SW (1991) Range perception through apparent image speed in freely flying honeybees. *Vis Neurosci* 6:519–535
- Srinivasan M V, Zhang SW (1997) Visual control of honeybee flight. *Orientation and communication in arthropods* 95–113
- Srinivasan, M. V., & Lehrer, M. (1988). Spatial acuity of honeybee vision and its spectral properties. *Journal of Comparative Physiology A*, 162, 159–172
- Srinivasan M V, Zhang SW, Lehrer M, Collett TS (1996) Honeybee navigation en route to the goal: visual flight control and odometry. *Journal of Experimental Biology* 199:237–244

Tammero LF, Dickinson MH (2002) Collision-avoidance and landing responses are mediated by separate pathways in the fruit fly, *Drosophila melanogaster*. *Journal of Experimental Biology* 205:2785–2798

Wallace GK (1959) Visual scanning in the desert locust *Schistocerca gregaria* Forskål. *Journal of Experimental Biology* 36:512–525

Figures

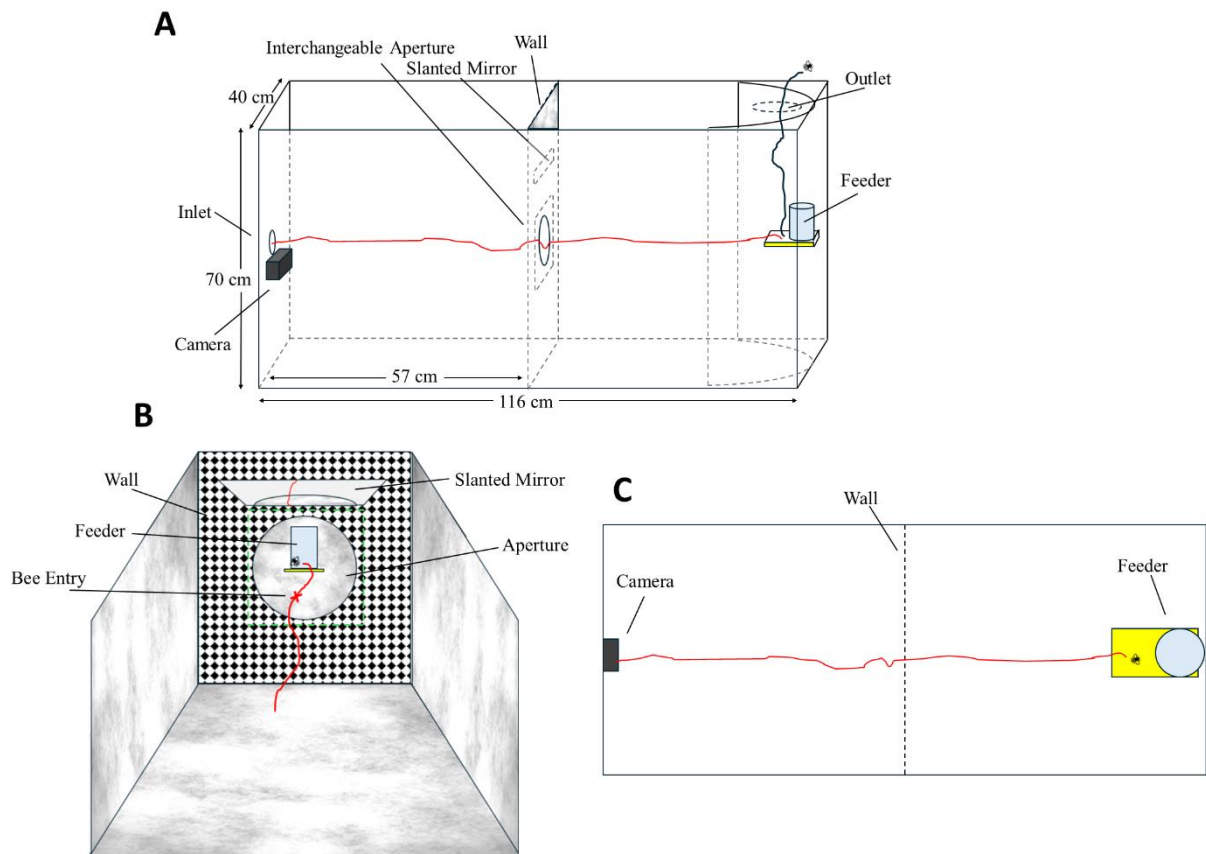


Figure 1: Layout of the experimental tunnel setup. (A) Side view showing bees entering through the inlet and flying toward the feeder (flight path indicated by the red line). The bees pass through an interchangeable aperture located on the central wall. (B) Front view of the wall from the camera's perspective, showing the checkerboard pattern surrounding the aperture and the slanted mirror mounted above. (C) Plan view of the setup, displaying a typical bee trajectory in red.

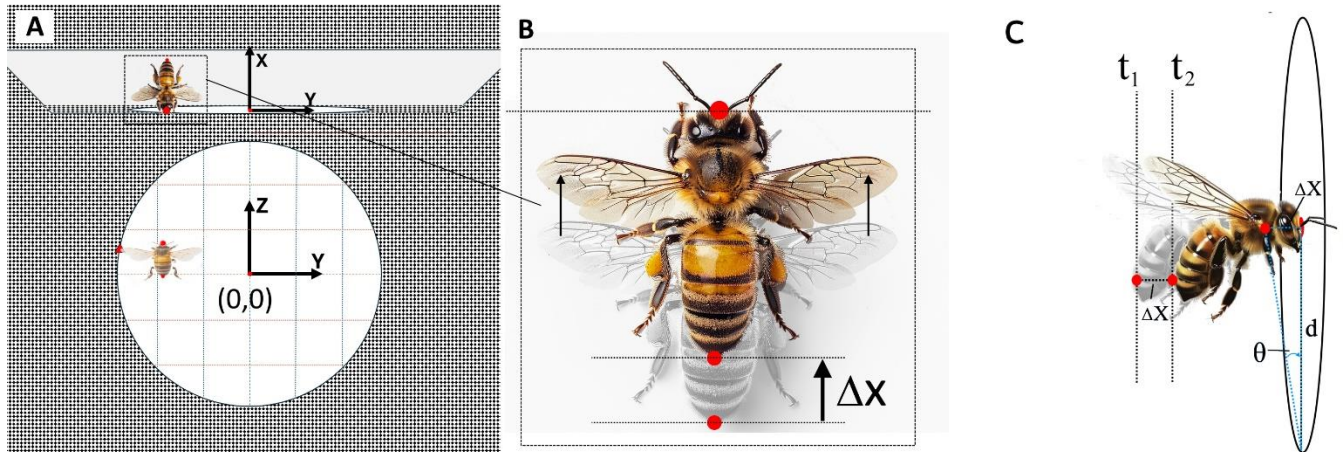


Figure 2: Illustration of the main viewing frames and the layout for digitisation of bee coordinates. A) shows both the frontal view and the top-down view through the mirror (the camera frame), with the coordinate system axes represented as black arrows, and the origin and an example point marked in red. In B), the image shows the rear tip of bee abdomens tracked manually in consecutive frames of the mirror view for estimating forward speed (the greyed-out bee is the original position). C) Schematic side view showing how the optic flow was constructed from the visual angle of the lowermost aperture edge subtended on the bee retina. The example shows the calculation using the bottom edge of the aperture. The time t_1 represents the frame before entry, and t_2 is the frame of entry (when the bee crosses the YZ plane).

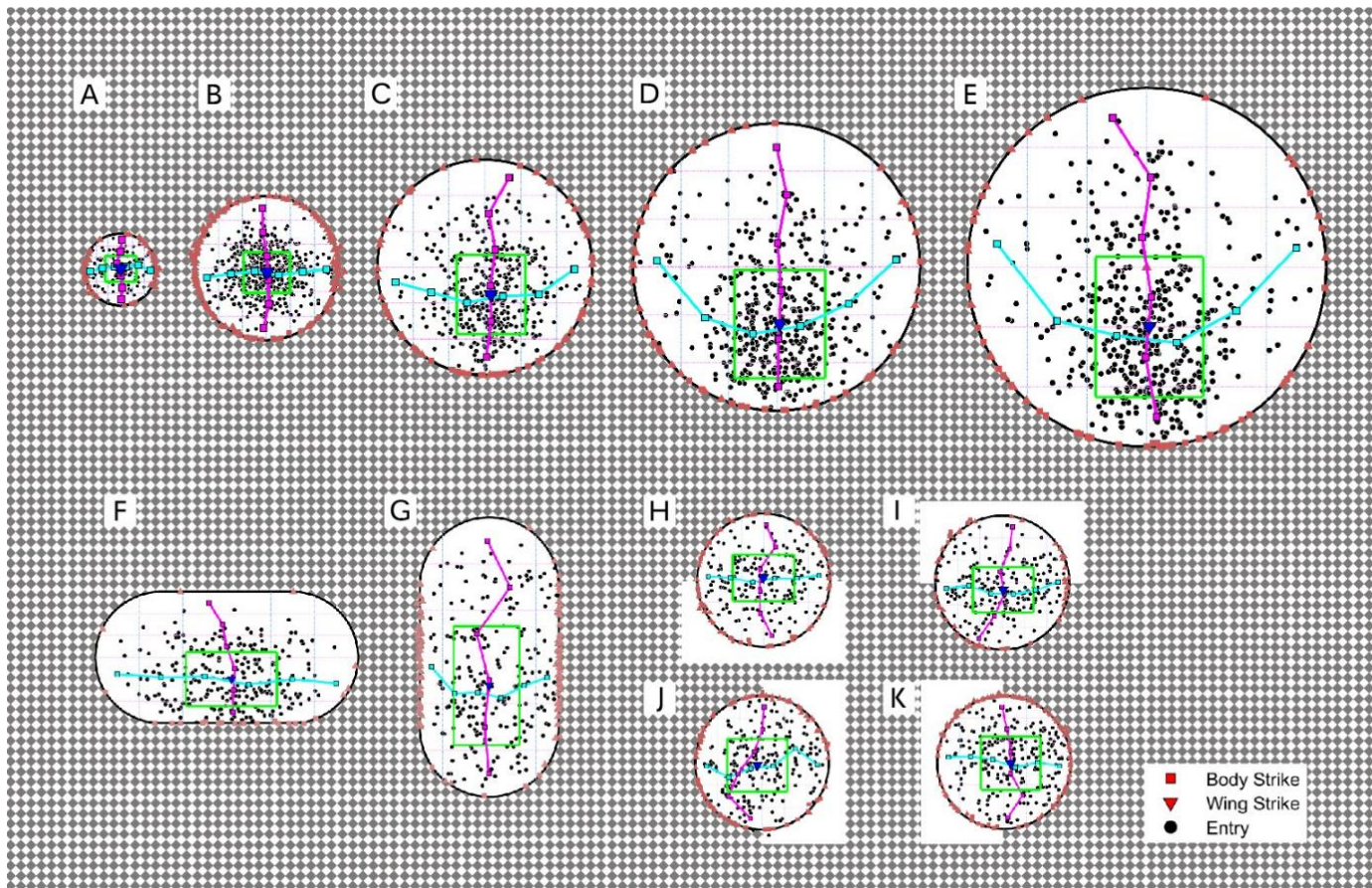


Figure 3: Visualization of entry and collision locations across all tested aperture shapes and sizes. Black markers indicate entry locations, while red markers represent collision points. The green boxes show the standard deviations of bee entry positions in both the horizontal and vertical directions. The six equi-spaced horizontal (blue) and vertical (magenta) bins are delineated by dotted lines, with square markers indicating the median entry location within each bin. The overall median entry location for each aperture is represented by a blue triangular marker. Thick magenta lines show the median horizontal positions, and thick cyan lines show the median vertical positions within each bin. The aperture shapes are scaled relative to one another and the actual relative size of the background pattern.

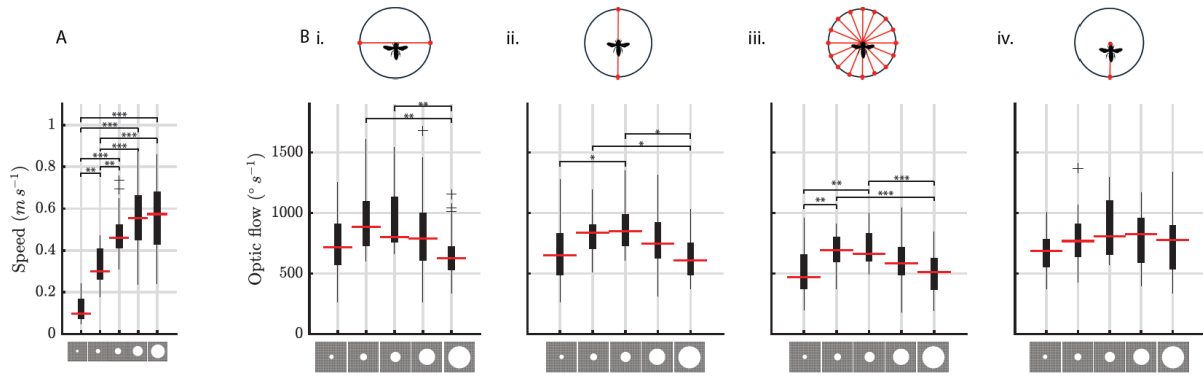


Figure 4: Boxplots of traversal speed (A) and optic flow (B) for all circular apertures with constant surrounding texture. Speed is measured in the longitudinal direction (X) of the tunnel setup. Optic flow results display the bilateral optic flow (Ω_{BL}) (B.i), the dorsoventral optic flow (Ω_{DV}) (B.ii), the total radial optic flow (Ω_R) (B.iii), and the ventral optic flow (Ω_V) (B.iv). Each optic flow metric is compared across apertures of different diameters (30–150 mm) with the median marked in red. The boxplots show outliers with the + symbol. Statistical significance between groups is indicated by asterisks ($p < 0.05$, $p < 0.01$, $p < 0.001$). The icons beneath the axes show the corresponding aperture patterns for each group. Sample sizes (n) and variability statistics for each set correspond to the metrics shown in Table 2.

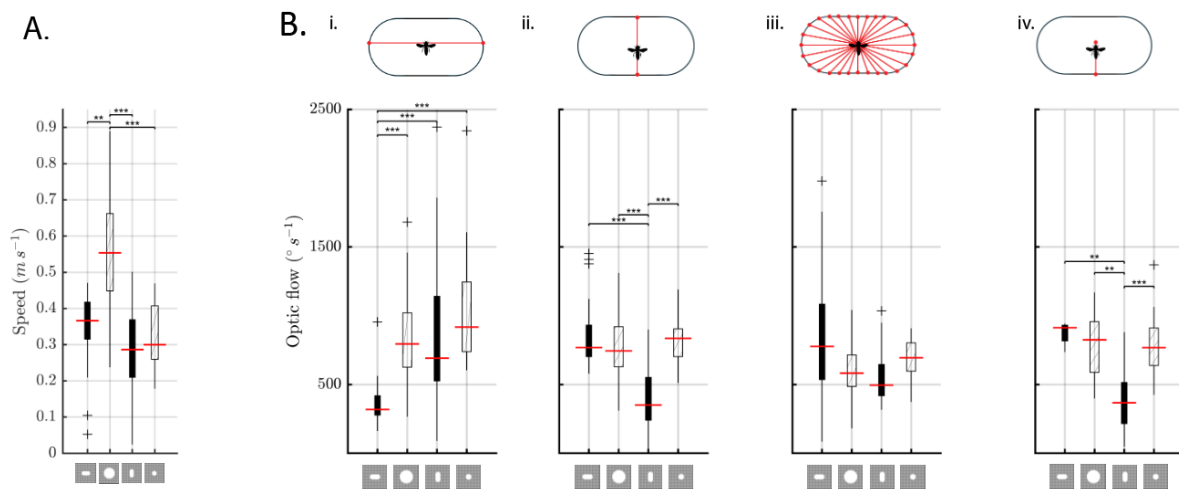


Figure 5: Boxplots of traversal speed (A) and optic flow (B) for both elongated apertures. Speed is measured in the longitudinal direction of the tunnel setup (X). Results include the bilateral OF (Ω_{BL}) (B.i), dorsoventral OF (Ω_{DV}) (B.ii), radial OF (Ω_R) (B.iii), and ventral OF (Ω_V) (B.iv). Each optic flow metric is compared across apertures, with the median marked in red. The boxplots display the median, interquartile range, and potential outliers. Statistical significance between groups is indicated by asterisks ($p < 0.05^*$, $p < 0.01^{**}$, $p < 0.001^{***}$). The icon bar underneath the axis shows the corresponding aperture patterns for each group.

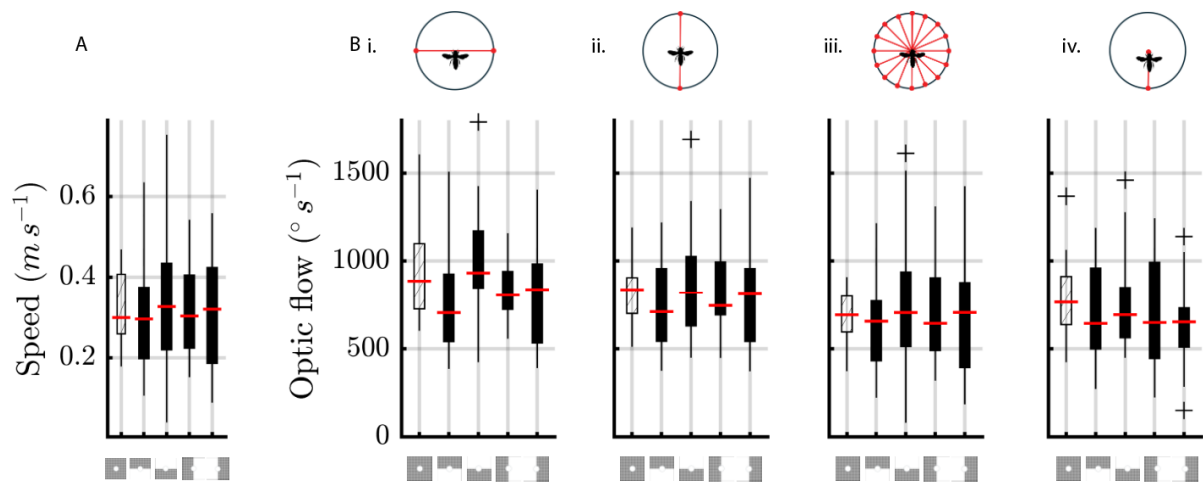


Figure 6: Boxplots of traversal speed (A) and optic flow (Bi-iv) for apertures with varying regions of texture flanking the 60 mm diameter circular aperture. Speed is measured in the longitudinal direction of the tunnel setup (X). Results include the bilateral OF (Ω_{BL}) (B.i) the dorsoventral OF (Ω_{DV}) (B.ii); the total OF (Ω_R) (B.iii); and the ventral OF (Ω_V) (B.iv). For comparison, the results of aperture B (60 mm diameter) are included. No significance was detected following group comparison tests.

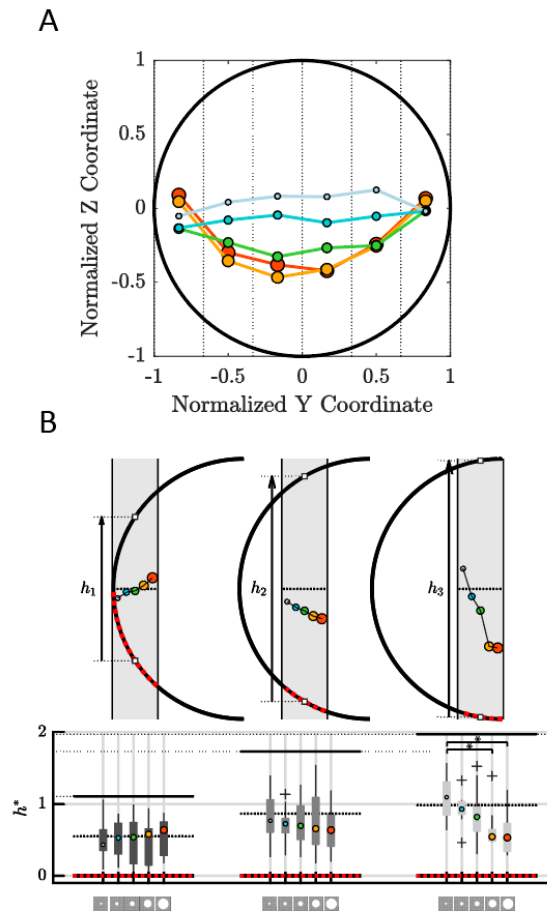


Figure 7: The three lateral entry location bins (outer, middle and inner) for the circular apertures of varying diameter. A) Shows the geometry of the aperture bins and displays a curve marking the height (measured vertically from the intersection with the edge below) relative to the shape. A marker in the middle of each bin is shown to reference the point where heights are measured. In B), the normalized heights above the edge vertically below (h_E^*) for all entry points are shown in box and whisker plots. Horizontal green lines represent the height in each bin, measured from the middle point. A) The median Z entry locations in each of the six laterally spaced bins for all five circular apertures of varying diameter. The coordinates are plotted in normalized units, where the radius of each circle is 1 in both directions. Solid lines are plotted between the medians for each diameter and overlaid on the same axes. The normalised total medians (calculated using all points, regardless of Y location) are displayed as circular markers. Significance was tested across all groups, shown by significance markers between relevant box-whisker plots. See Table S12 and S13 for full comparison statistics.

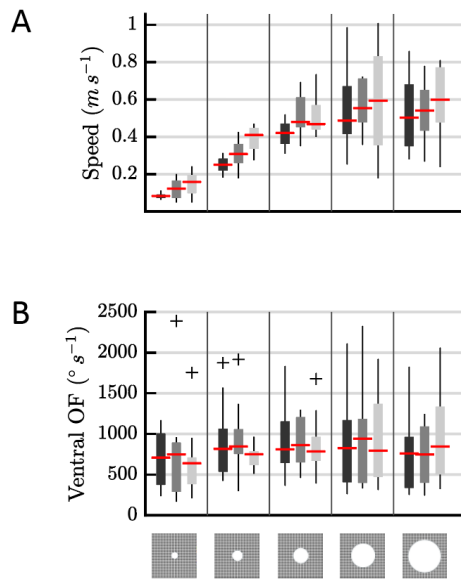


Figure 8: Boxplots of bee entry speed (v_x) (A) and ventral OF (Ω_v) (B) in each lateral bin of each of the circular apertures. Data for each aperture are separated into three lateral regions of entry, labeled ‘Inner’, ‘Middle’, and ‘Outer’ as illustrated in Fig. 7. The boxplots show the median (red line), interquartile range, and outliers, with corresponding aperture configuration icons below the plots.

Tables

Table 1: Spatial statistics for the position samples from of all tested shapes and sizes shown in Fig. 3. Aperture widths (in mm), the number of samples recorded, the median horizontal (\bar{Y}) and vertical (\bar{Z}) coordinates (in mm) are displayed for each aperture type (A–K). The table provides the MAD for Y and Z coordinates, the number of collisions recorded, the collision ratio ($N_{\text{Collisions}}/N_{\text{Entries}}$), and the wing strike ratio ($N_{\text{Collisions}}/N_{\text{Wing Collisions}}$) for each aperture.












Label	A	B	C	D	E	F	G	H	I	J	K
Type											
Width (mm)	30	60	90	120	150	120	60	60	60	60	60
Samples	109	534	385	456	446	260	236	204	191	223	199
Median horizontal coordinate \bar{Y} (mm)	0.21	0.17	2.51	1.25	1.06	2.21	-0.04	-0.12	0.41	-3.01	2.07
Median vertical coordinate \bar{Z} (mm)	0.24	-1.87	-11.40	-23.84	-24.89	-9.88	-12.31	1.09	-3.22	-0.38	-0.99
MAD _Y (mm)	5.53	7.61	10.96	14.63	16.99	15.36	14.17	10.93	10.79	9.89	10.04
MAD _Z (mm)	4.49	6.75	13.57	18.69	23.79	10.46	23.41	7.51	9.01	9.44	10.15
Collisions	67	149	70	55	46	25	120	98	94	116	105
Collision ratio	0.615	0.279	0.182	0.121	0.103	0.096	0.508	0.480	0.492	0.520	0.528
Wing strike ratio	0.967	0.981	0.513	0.429	0.177	0.332	0.938	0.770	0.898	0.885	0.888

Table 2. Median comparisons for speed and OF metrics from circular aperture traversals of varying diameters (30–150 mm). The table presents the median, coefficient of variation based on the median (CV_{Med}), median absolute deviation (MAD), interquartile range (IQR), range, and group comparison (KW) p-values for each optic flow metric: speed (v_x), bilateral OF (Ω_{BL}), dorsoventral OF (Ω_{DV}), total radial OF (Ω_{R}), and ventral OF (Ω_{V}). Statistical significance of differences across aperture sizes is indicated by the group-level (KW) p-values, which are based on the complete datasets. The complete statistical details of the datasets shown here can be found in Tables S1, S4, and S6.

Label	Metric	n	Median	CV_{Med}	MAD	IQR	Range	Group-Level Comparison (p)
A-E	v_x	150	0.4615	0.244	0.1124	0.3094	0.4763	<0.0001
A-E	Ω_{BL}	116	788.5	0.092	72.3	127.5	259.3	0.0008
A-E	Ω_{DV}	118	744.7	0.1294	96.4	200.03	240.6	0.0002
A-E	Ω_{R}	116	582.4	0.136	79.2	168.2	223.5	<0.0001
A-E	Ω_{V}	111	778.44	0.0398	31	65.70	136.8	0.2387

Table 3: Summary table presenting the results of pairwise multiple comparisons of median entry locations for varying flanked texture positions. The pairwise comparisons (Dunn’s test) evaluate differences in Y and Z coordinates between the control (B) and the texture-flanked apertures (H, I, J), categorized by vertical and horizontal flanking. The complete Dunn’s test results are shown in the upper-triangle tables in Figures S9 and S10. See Table S5 and S8 for the full results of the non-parametric group-level comparison (KW H test).

Pairwise Comparison	Metric	Absolute difference (mm)	Pairwise Comparison (p)
Control (B) vs H (Upper flanked)	$\Delta\tilde{Y}$	-0.29	0.9703
	$\Delta\tilde{Z}$	2.13	0.2834
Control (B) vs I (Lower flanked)	$\Delta\tilde{Y}$	0.24	0.9042
	$\Delta\tilde{Z}$	-2.96	0.5177
H vs I (Upper vs. lower flank)	$\Delta\tilde{Y}$	0.53	0.8384
	$\Delta\tilde{Z}$	-4.31	0.1004
Control (B) vs J (Left flanked)	$\Delta\tilde{Y}$	-3.18	0.0662
	$\Delta\tilde{Z}$	1.49	0.2834
Control (B) vs K (Right flanked)	$\Delta\tilde{Y}$	1.9	0.1029
	$\Delta\tilde{Z}$	0.88	0.5177
J vs K (Left vs. right flank)	$\Delta\tilde{Y}$	5.08	0.0036**
	$\Delta\tilde{Z}$	0.61	0.0036**

Table 4. Summary of statistics for the medians of speed and optic flow metrics for 60 mm diameter pattern-flanked circular apertures of varying diameters (30–150 mm). The table presents the coefficient of variation based on the medians (CV_{Med}), median absolute deviation (MAD), interquartile range (IQR), and range for the medians of each optic flow metric: speed (V_x), bilateral OF (Ω_{BL}), dorsoventral OF (Ω_{DV}), total radial OF (Ω_R), and ventral OF (Ω_V). The group-level comparison p-value is based on the results of the KW tests on the complete datasets. Full statistical details can be found in Table S3.

Label	Metric	Median	CV_{Med}	MAD	IQR	Range	Group-Level Comparison (p)
B, H-K	V_x	0.3039	0.0240	0.0073	0.0233	0.0306	0.8885
B, H-K	Ω_{BL}	884.3	0.0584	51.6	149.15	228.8	0.0716
B, H-K	Ω_{DV}	815.2	0.0240	19.60	82.06	122.12	0.3179
B, H-K	Ω_R	694.10	0.0200	13.90	52.70	62.30	0.7540
B, H-K	Ω_V	654	0.0131	8.60	63.88	122	0.1490

Supplementary Information

Table S1: Summary of visual flow statistics for circular apertures of varying diameters. The table includes the median speed (v_x), interquartile range (IQR), median absolute deviation (MAD), and coefficient of variation based on the median (CV_{Med}) for each aperture size (A–E). Group-level comparison p-values (KW test outputs) are included to indicate the statistical significance of differences across aperture sizes.

Label	Type	Metric	n	Median	IQR	MAD	CV_{Med}	Group-Level Comparison (p)
A		v_x	30	0.0976	0.0780	0.0301	0.3085	-
B			30	0.2999	0.1475	0.0615	0.2049	
C			30	0.4580	0.1120	0.0528	0.1153	
D			30	0.5536	0.2134	0.1085	0.1960	
E			30	0.5739	0.2507	0.1323	0.2306	
A-E	30-150 mm	v_x	150	0.4131	0.3195	0.1607	0.3889	<0.0001
A		Ω_{BL}	24	716.19	336.48	181.16	0.2529	-
B			24	884.34	370.04	174.21	0.1970	
C			21	799.79	378.79	71.14	0.0889	
D			23	788.49	395.87	189.03	0.2397	
E			24	625.00	188.57	94.283	0.1509	
A-E	30-150 mm	Ω_{BL}	116	770.28	346.26	167.12	0.2170	0.0008
A		Ω_{DV}	24	648.34	345.69	168.67	0.2602	-
B			25	834.82	201.49	85.512	0.1024	
C			23	847.7	261.04	128.97	0.1521	
D			22	744.71	292.36	120.82	0.1622	
E			24	607.14	267.25	126.98	0.2091	
A-E	30-150 mm	Ω_{DV}	118	743.25	278.45	136.93	0.1842	0.0002
A		Ω_R	24	470.57	280.79	133.18	0.2830	-
B			22	694.14	205.83	104.10	0.1500	
C			23	661.59	226.84	90.684	0.1371	
D			24	582.42	229.75	121.27	0.2082	
E			23	511.82	261.05	128.41	0.2509	
A-E	30-150 mm	Ω_R	116	606.40	248.07	131.22	0.2164	<0.0001
A		Ω_V	21	687.84	226.26	131.10	0.1906	-
B			24	767.44	272.55	140.12	0.1826	
C			24	809.37	449.01	158.46	0.1958	
D			22	824.61	369.62	158.37	0.1921	
E			20	778.44	361.77	176.78	0.2271	
A-E	30-150 mm	Ω_V	111	767.43	281.45	146.37	0.1907	0.2387

Table S2: Visual flow statistics for elongated apertures. The table presents the median, interquartile range (IQR), median absolute deviation (MAD), coefficient of variation based on the median (CV_{Med}), and p-values for pairwise comparisons (MW) of each OF metric: speed (v_x), bilateral OF (Ω_{BL}), dorsoventral OF (Ω_{DV}), total radial OF (Ω_R), and ventral OF (Ω_V). Pairwise comparisons (using the MW U test) were used here, with p-values <0.05 indicating significant differences across these groups.












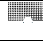








Label	Type	Metric	n	Median	IQR	MAD	CV_{Med}	Pairwise Comparison (p)
F		v_x	30	0.366	0.1046	0.0523	0.1429	-
G			30	0.143	0.0895	0.0477	0.3333	
F-G	-	v_x	60	0.215	0.2439	0.1101	0.5128	<0.0001
F		Ω_{BL}	23	316.98	170.02	64.86	0.2046	-
G			25	213.01	151.02	75.64	0.3551	
F-G	-	Ω_{BL}	48	267.77	169.95	84.97	0.3173	0.0026
F		Ω_{DV}	22	486.44	322.96	113.69	0.2337	-
G			25	89.18	83.74	46.38	0.5201	
F-G	-	Ω_{DV}	47	163.61	325.29	128.24	0.7838	<0.0001
F		Ω_R	22	806.26	433.83	284.35	0.3527	-
G			25	310.24	225.76	112.47	0.3625	
F-G	-	Ω_R	47	449.75	528.33	259.95	0.5780	<0.0001
F		Ω_V	16	1143	889.99	420.16	0.3677	-
G			17	193.58	230.28	104.74	0.5411	
F-G	-	Ω_V	33	339.36	691.66	243.05	0.7162	0.0001

Table S3: Summary statistics of visual flow for 60 mm diameter circular apertures with different flanked texture configurations. The table includes the median, IQR, MAD, and CV_{Med} for each group. Statistical comparisons across groups were conducted using the KW H-test, with group-level p-values reported in the final column. Combined statistics for all groups (B, H–K) are also provided.

Label	Type	Metric	n	Median	IQR	MAD	CV_{Med}	Group-Level Comparison (p)
B		v_x	30	0.2999	0.1475	0.0615	0.2049	-
H			30	0.2966	0.1801	0.0847	0.2857	
I			30	0.3272	0.2181	0.1091	0.3333	
J			30	0.3039	0.1846	0.0868	0.2857	
K			30	0.3208	0.2413	0.1138	0.3548	
B, H-K	-	v_x	150	0.3105	0.1906	0.0950	0.3061	0.8885
B		Ω_{BL}	24	917.52	507.36	198.51	0.2163	-
H			22	713.99	445.41	206.70	0.2895	
I			22	959.04	538.26	191.43	0.1996	
J			21	817.54	269.06	124.21	0.1519	
K			23	859.17	382.21	162.68	0.1893	

B, H-K	-	Ω_{BL}	112	842.05	297.40	148.50	0.1764	0.0716
B		Ω_{DV}	24	852.28	205.48	99.91	0.1172	-
H			20	712.68	420.80	188.42	0.2644	
I			21	833.24	502.76	202.65	0.2432	
J			22	747.98	308.79	123.02	0.1645	
K			21	815.22	421.16	181.12	0.2222	
B, H-K	-	Ω_{DV}	108	816.46	347.82	177.68	0.2176	0.3179
B		Ω_R	25	694.13	205.83	104.10	0.1500	-
H			23	657.68	349.67	209.69	0.3188	
I			26	707.24	430.85	207.68	0.2937	
J			27	645.74	421.04	178.33	0.2762	
K			26	707.95	489.63	231.10	0.3264	
B, H-K	-	Ω_R	127	677.42	369.81	185.53	0.2739	0.7540
B		Ω_V	24	775.93	288.29	150.66	0.1942	-
H			22	645.40	467.38	260.68	0.4039	
I			23	727.71	775.60	193.37	0.2657	
J			23	650.42	555.60	225.59	0.3468	
K			22	654.03	232.02	117.78	0.1801	
B, H-K	-	Ω_V	114	703.03	414.63	198.48	0.2823	0.1490

Table S4: Group comparison test results for circular aperture group comparisons across various OF metrics. The table displays the number of samples (n), H-statistic (χ^2), KW p-values for the overall comparison of groups, and significant Dunn's post-hoc pairwise comparisons for speed, bilateral OF (Ω_{BL}), dorsoventral OF (Ω_{DV}), radial OF (Ω_R), and ventral OF (Ω_V). Significant Dunn comparisons are indicated with asterisks: $p < 0.05$ (*), $p < 0.01$ (**), and $p < 0.001$ (***). NS indicates non-significant results. There are four degrees of freedom.

Label	Metric	n	H-Statistic (χ^2)	Group-Level Comparison (p)	Effect size (η)	Significant Pairwise Comparisons (p)
A-E	v_x	150	94.79	<0.0001	0.71	A vs B (p = 0.0040)**
						A vs C (p = 0.0000)***
						A vs D (p = 0.0000)***
						A vs E (p = 0.0000)***
						B vs C (p = 0.0083)**
						B vs D (p = 0.0001)***
A-E	Ω_{BL}	116	18.84	0.0008	0.12	B vs E (p = 0.0046)**
						C vs E (p = 0.0073)**
						A vs C (p = 0.0105)*
A-E	Ω_{DV}	118	21.71	0.0002	0.14	B vs E (p = 0.0151)*
						C vs E (p = 0.0012)**
						A vs B (p = 0.0020)**
A-E	Ω_R	116	30.6	<0.0001	0.21	A vs C (p = 0.0010)**
						B vs E (p = 0.0009)***
						C vs E (p = 0.0004)***
						NS
A-E	Ω_V	111	5.51	0.2387	0.01	NS

Table S5: Results for group comparisons (KW) across OF metrics corresponding to 60 mm circular apertures with varying positions of flanked texture. The table displays the number of samples (n), and the output from the nonparametric group comparison test (KW): the H-statistic (χ^2), p-value and effect size (ϵ^2). Any significant Dunn's post-hoc pairwise comparisons are shown for speed (v_x), bilateral OF (Ω_{BL}), dorsoventral OF (Ω_{DV}), radial OF (Ω_R), and ventral OF (Ω_V). NS indicates non-significant results. There are four degrees of freedom (df).

Label	Metric	n	H-Statistic (χ^2)	Group-Level Comparison (p)	Effect Size (ϵ^2)	Significant Pairwise Comparisons (p)
B, H-K	v_x	150	1.14	0.8885	-0.0225	All NS
B, H-K	Ω_{BL}	112	8.61	0.0716	0.0518	All NS
B, H-K	Ω_{DV}	108	4.71	0.3179	0.0072	All NS
B, H-K	Ω_R	127	1.9	0.754	-0.0165	All NS
B, H-K	Ω_V	114	6.76	0.149	0.0279	All NS

Table S6: Statistical comparisons of OF metrics for circular apertures (A-E) using Dunn's post-hoc test following significant group comparison tests (KW). The p-value, effect size (r), estimated difference (Δ) and confidence interval (CI) is reported for each pairwise comparison. Δ and CI are rank-based and therefore have units in mean ranks. OF metrics include speed (v_x), bilateral OF (Ω_{BL}), dorsoventral OF (Ω_{DV}), and radial optic flow (Ω_R). Ventral OF (Ω_V) is excluded as group-level comparison tests did not yield significant p-values for this metric. Significant comparisons are indicated by p-values (p < 0.05 (*), p < 0.01 (**), p < 0.001 (***)).

Metric	Label	A	B	C	D	E	
v_x	A	-	$p_{adj} = 0.0040^{**}$	$p_{adj} = 0.0000^{**}$	$p_{adj} = 0.0000^{**}$	$p_{adj} = 0.0000^{**}$	
			$r = -0.5233$	$r = -0.5426$	$r = -0.5366$	$r = -0.5414$	
			$\Delta = -39.83$ CI = [-71.24, -8.43]	$\Delta = -78.23$ CI = [-109.6, -46.83]	$\Delta = -89.20$ CI = [-120.6, -57.80]	$\Delta = -89.07$ CI = [-120.47, -57.66]	
	B	-	-	$p_{adj} = 0.0083^{**}$	$p_{adj} = 0.0001^{**}$	$p_{adj} = 0.0000^{**}$	
				$r = -0.4267$	$r = -0.3917$	$r = -0.4074$	
				$\Delta = -38.40$ CI = [-69.80, -6.99]	$\Delta = -49.37$ CI = [-80.77, -17.96]	$\Delta = -49.23$ CI = [-80.64, -17.83]	
	C	-	-	-	-	$p_{adj} = 0.8729$	$p_{adj} = 0.9472$
						$r = -0.1491$	$r = -0.1334$
						$\Delta = -10.97$ CI = [-42.37, 20.44]	$\Delta = -10.83$ CI = [-42.24, 20.57]
	D	-	-	-	-	-	$p_{adj} = 1.0000$
							$r = -0.0042$
							$\Delta = 0.13$ CI = [-31.27, 31.53]

	E	-	-	-	-	-	
Ω_{BL}	A	-		$p_{adj} = 0.0953$	$p_{adj} = 0.9556$	$p_{adj} = 0.9556$	$p_{adj} = 0.9902$
				$r = -0.2380$	$r = -0.2430$	$r = -0.1041$	$r = 0.0706$
				$\Delta = -23.76$	$\Delta = -24.40$	$\Delta = -10.10$	$\Delta = 8.17$
				$CI = [-49.58, 2.05]$	$CI = [-51.69, 2.89]$	$CI = [-35.62, 15.41]$	$CI = [-17.35, 33.69]$
	B	-	-		$p_{adj} = 1.0000$	$p_{adj} = 0.7628$	$p_{adj} = 0.0046$
					$r = 0.0000$	$r = 0.1568$	$r = 0.3388$
					$\Delta = -0.64$	$\Delta = 13.66$	$\Delta = 31.93$
	C	-	-	-	$CI = [-27.93, 26.65]$	$CI = [-11.86, 39.18]$	$CI = [6.41, 57.45]$
					$p_{adj} = 0.7743$	$p_{adj} = 0.0073$	
					$r = 0.1186$	$r = 0.3586$	
	D	-	-	-	$\Delta = 14.30$	$\Delta = 32.57$	
					$CI = [-12.71, 41.31]$	$CI = [5.56, 59.58]$	
					$p_{adj} = 0.3524$	$p_{adj} = 0.1908$	
	E	-	-	-	$r = 0.1908$	$r = 0.1908$	
					$\Delta = 18.27$	$\Delta = 18.27$	
$CI = [-6.95, 43.49]$					$CI = [-6.95, 43.49]$		
Ω_{DV}	A	-		$p_{adj} = 0.0907$	$p_{adj} = 0.0105$	$p_{adj} = 0.6994$	$p_{adj} = 0.9996$
				$r = -0.2358$	$r = -0.2880$	$r = -0.1534$	$r = 0.0429$
				$\Delta = -25.31$	$\Delta = -31.59$	$\Delta = -15.45$	$\Delta = 5.94$
				$CI = [-52.63, 2.00]$	$CI = [-58.59, -4.58]$	$CI = [-42.76, 11.86]$	$CI = [-21.07, 32.94]$
	B	-	-		$p_{adj} = 0.9994$	$p_{adj} = 0.9796$	$p_{adj} = 0.0151$
					$r = -0.0712$	$r = 0.0956$	$r = 0.3073$
					$\Delta = -6.27$	$\Delta = 9.86$	$\Delta = 31.25$
	C	-	-	-	$CI = [-33.87, 21.33]$	$CI = [-18.03, 37.76]$	$CI = [3.66, 58.85]$
					$p_{adj} = 0.6577$	$p_{adj} = 0.0012$	
					$r = 0.1606$	$r = 0.3518$	
	D	-	-	-	$\Delta = 16.1344$	$\Delta = 37.52$	
					$CI = [-11.46, 43.73]$	$CI = [10.23, 64.81]$	
					$p_{adj} = 0.2628$	$p_{adj} = 0.2073$	
	E	-	-	-	$r = 0.2073$	$r = 0.2073$	
					$\Delta = 21.39$	$\Delta = 21.39$	
$CI = [-6.21, 48.98]$					$CI = [-6.21, 48.98]$		
Ω_R	A	-		$p_{adj} = 0.0020$	$p_{adj} = 0.0010$	$p_{adj} = 0.7269$	$p_{adj} = 1.0000$
				$r = -0.2789$	$r = -0.3141$	$r = -0.1337$	$r = -0.0043$
				$\Delta = -41.17$	$\Delta = -43.03$	$\Delta = -17.43$	$\Delta = 2.13$
				$CI = [-72.15, -10.18]$	$CI = [-74.02, -12.05]$	$CI = [-48.97, 14.10]$	$CI = [-28.85, 33.12]$
	B	-	-		$p_{adj} = 1.0000$	$p_{adj} = 0.3006$	$p_{adj} = 0.0009$
					$r = 0.0018$	$r = 0.1708$	$r = 0.3336$
					$\Delta = -1.87$	$\Delta = 23.73$	$\Delta = 43.30$
	C	-	-	-	$CI = [-32.85, 29.12]$	$CI = [-7.80, 55.27]$	$CI = [12.31, 74.29]$
					$p_{adj} = 0.2080$	$p_{adj} = 0.0004$	
					$r = 0.1938$	$r = 0.3397$	
	D	-	-	-	$\Delta = 25.60$	$\Delta = 45.17$	
					$CI = [-5.94, 57.14]$	$CI = [14.18, 76.15]$	
					$p_{adj} = 0.5767$	$p_{adj} = 0.1413$	
	E	-	-	-	$r = 0.1413$	$r = 0.1413$	
					$\Delta = 19.57$	$\Delta = 19.57$	
$CI = [-11.97, 51.10]$					$CI = [-11.97, 51.10]$		

Table S7: Observed collision counts for the five texture location groups: Control (uniform texture), Top Flanked, Bottom Flanked, Left Flanked, and Right Flanked, measured across four edges of the aperture (Left, Right, Upper, and Lower).

	Left Edge	Right Edge	Upper Edge	Lower Edge
Control	53	56	55	54
Top Flanked	35	26	30	31
Bottom Flanked	23	26	25	24
Left Flanked	36	20	24	32
Right Flanked	19	32	20	31

Table S8: Comparison of median differences in Y and Z coordinates between the control (B) and texture-flanked apertures (H–K), as well as between apertures flanked with texture on opposite sides in the vertical and horizontal directions. The table presents the group comparison (KW) H-statistic and corresponding p-values, along with significant pairwise comparisons from Dunn’s post-hoc tests ($p < 0.05$). There are two degrees of freedom (df) for the group comparisons.



Comparison	Metric	n	H-statistic	Group-Level Comparison (p)	Effect Size (ϵ^2)	Significant Pairwise Comparisons (p)
 B, H-I	Y coordinate	637	0.57	0.7502	0.00	All NS
	Z coordinate		4.55	0.1030	0.00	All NS
 B, J-K	Y coordinate	635	10.49	0.0053	0.02	J vs K ($p = 0.0036$)
	Z coordinate		4.67	0.0969	0.01	All NS

Table S9: Upper triangle tables displaying post-hoc pairwise test (Dunn’s) results for the comparison of Y and Z coordinates between the control (aperture B, 60 mm diameter) and the texture-flanked apertures (H, I) in the vertical flanking configuration. The p-values, effect sizes (r), estimated differences (Δ) and confidence intervals (CI) are reported for each pairwise comparison. Δ and CI are rank-based and therefore have units in mean ranks.

Metric	Label	B	H	I	
Y coord	B	-	$p_{adj} = 0.9703$	$p_{adj} = 0.9042$	
			$r = 0.0205$	$r = -0.0280$	
			$\Delta = -9.37$	$\Delta = 13.07$	
			CI = [-61.20, 42.46]	CI = [-40.16, 66.32]	
	H	-	-	$p_{adj} = 0.8384$	
				$r = -0.0393$	
$\Delta = 22.45$					
			CI = [-48.55, 93.44]		
I	-	-	-	-	
Z coord	B	-	$p_{adj} = 0.2834$	$p_{adj} = 0.5177$	
			$r = -0.0658$	$r = 0.0507$	
			$\Delta = -42.95$	$\Delta = 33.69$	
			CI = [-106.23, 20.34]	CI = [-31.30, 98.68]	
	H	-	-	$p_{adj} = 0.1004$	
				$r = 0.0707$	
				$\Delta = 76.64$	
				CI = [-9.99, 163.27]	
	I	-	-	-	-

Table S10: Upper triangle tables displaying post-hoc pairwise test (Dunn’s) results for the comparison of Y and Z coordinates between the control (Aperture B, 60 mm) and the texture-flanked apertures (J, K) in the horizontal flanking configuration. The p-values, effect sizes (r), difference estimates (Δ), and confidence intervals are reported for each pairwise comparison. Δ and CI are rank-based and therefore have units in mean ranks.

Metric	Label	B	J	K	
Y coord	B	-	$p_{adj} = 0.0662$	$p_{adj} = 0.1029$	
			$r = 0.1121$	$r = -0.1059$	
			$\Delta = 49.11$	$\Delta = -46.93$	
			CI = [-3.29, 101.51]	CI = [-100.04, 6.19]	
	J	-	-	$p_{adj} = 0.0036$	
				$r = -0.1290$	
$\Delta = -96.04$					
			CI = [-167.36, -24.70]		
K	-	-	-	-	
Z coord	B	-	$p_{adj} = 0.2834$	$p_{adj} = 0.5177$	
			$r = -0.0208$	$r = -0.0953$	
			$\Delta = -9.63$	$\Delta = -43.40$	
			CI = [-62.02, 42.76]	CI = [-96.52, 9.72]	
	J	-	-	$p_{adj} = 0.1004$	
				$r = -0.0503$	
$\Delta = -33.77$					
			CI = [-105.11, 37.56]		

	K	-	-	-
--	---	---	---	---

Table S11: Normalized centering metrics for circular apertures of varying diameters (30-150 mm). The table shows the median and MAD of the Y and Z coordinates, normalized by aperture size (diameter), across different aperture types (A–E).






Label	Aperture type	Diameter (mm)	Normalised Median Y Coordinate	Normalised Median Z Coordinate	Normalised MAD Y Coordinate	Normalised MAD Z Coordinate
A		30	1.40	1.60	0.37	0.30
B		60	0.56	-6.22	0.25	0.23
C		90	5.59	-25.24	0.24	0.15
D		120	2.08	-39.74	0.24	0.31
E		150	1.42	-33.19	0.23	0.32

Table S12: Normalized segment heights, bee centering metrics, and rank-based one-way KW test results for height datasets in each aperture segment, corresponding to the boxplots in Fig. 7B. The table includes absolute sector height (h), normalized height centering ratios (h_E^*/h^*), and group comparisons (KW) of height above the lower edge p-values. Significant pairwise comparisons (following post-hoc tests, Table S13) are listed for aperture types where relevant.

Aperture segment trisector	Normalised Segment Height (h^*)	Diameter (mm)	Absolute Segment Height (h) (mm)	h_E^*	h_E^*/h^*	h_E^* Group-Level Comparison (p)	Significant Pairwise Comparisons
Inner	1.97	30	29.55	1.10	0.56	0.0045	A vs D ($p = 0.0288$) A vs E ($p = 0.0165$)
		60	59.10	0.93	0.47		
		90	88.65	0.82	0.42		
		120	118.20	0.54	0.27		
		150	147.75	0.53	0.27		
Middle	1.73	30	25.95	0.77	0.45	0.9422	All NS
		60	51.90	0.72	0.42		
		90	77.85	0.70	0.40		
		120	103.80	0.66	0.38		
		150	129.75	0.64	0.37		
Outer	1.11	30	16.65	0.43	0.39	0.9553	All NS
		60	33.30	0.53	0.48		
		90	49.95	0.54	0.49		
		120	66.60	0.58	0.52		
		150	83.25	0.64	0.58		

Table S13: Upper triangle comparisons of normalized height above edge (h_E^*) above the edge for inner aperture segments following the significant group comparison result shown in Table S12. Pairwise comparisons are displayed only for the inner segment as other segments were not significant. The table includes adjusted p-values (p_{adj}), effect sizes (r), mean differences (Δ), and confidence intervals (CI). Significant results are marked with an asterisk (*).

Category	Label	A	B	C	D	E
Inner	A	-	$p_{adj} = 0.9976$	$p_{adj} = 0.7703$	$p_{adj} = 0.0288^*$	$p_{adj} = 0.0165^*$
			$r = 0.1336$	$r = 0.2085$	$r = 0.4009$	$r = 0.4009$
			$\Delta = 4.9$	$\Delta = 9.7$	$\Delta = 19.4$	$\Delta = 20.5$
			CI = [-13.4, 23.2]	CI = [-8.6, 28.0]	CI = [1.1, 37.7]	CI = [2.2, 38.8]
	B	-	-	$p_{adj} = 0.9980$	$p_{adj} = 0.2327$	$p_{adj} = 0.1551$
				$r = 0.1336$	$r = 0.3154$	$r = 0.3154$
				$\Delta = 4.8$	$\Delta = 14.5$	$\Delta = 15.6$
				CI = [-13.5, 23.1]	CI = [-3.8, 32.8]	CI = [-2.7, 33.9]
	C	-	-	-	$p_{adj} = 0.7703$	$p_{adj} = 0.6419$
					$r = 0.2405$	$r = 0.2298$
					$\Delta = 9.7$	$\Delta = 10.8$
					CI = [-8.6, 28.0]	CI = [-7.5, 29.1]
	D	-	-	-	-	$p_{adj} = 1.0000$
						$r = 0.0588$
						$\Delta = 1.1$
						CI = [-17.2, 19.4]
E	-	-	-	-	-	

Table S14. Median comparisons for speed and OF metrics from elongated aperture traversals (F and G). Group comparison (KW) p-values for each OF metric: speed (v_x), bilateral OF (Ω_{BL}), dorsoventral OF (Ω_{DV}), total radial OF (Ω_R), and ventral OF (Ω_V). Statistically significant pairwise comparisons (Dunn's) are shown from the complete upper-triangle table displayed in Table S15.






Label	Aperture Type	Metric	n	H-Statistic (χ^2)	Group-Level Comparison (p)	Significant Pairwise Comparisons
F, D, G, B		v_x	120	38.15	<0.0001	F vs D (p = 0.0019)** D vs G (p = 0.0000)*** D vs B (p = 0.0000)***
F, D, G, B		Ω_{BL}	95	33.80	<0.0001	F vs D (p = 0.0020)** F vs G (p = 0.0001)*** F vs B (p = 0.0000)***
F, D, G, B		Ω_{DV}	94	29.10	<0.0001	F vs G (p = 0.0004)*** D vs G (p = 0.0003)*** G vs B (p = 0.0000)***
F, D, G, B		Ω_R	93	6.10	0.107	All NS
F, D, G, B		Ω_V	79	24.12	<0.0001	F vs G (p = 0.0004)*** D vs G (p = 0.0006)*** G vs B (p = 0.0003)***

Table S15: Upper triangle pairwise comparisons table for speed and optic flow metrics from elongated aperture traversals and relevant-diameter circular apertures (B, 60 mm and D, 120 mm). Adjusted p-values (p_{adj}), effect sizes (r), mean differences (Δ), and confidence intervals (CI) are presented for each metric: speed (v_x), bilateral OF (Ω_{BL}), dorsoventral OF (Ω_{DV}), and ventral OF (Ω_V). Significant results are indicated by $p_{adj} < 0.05$ and marked with an asterisk (*). CIs are included for all comparisons to provide a complete assessment of effect sizes and their variability.

Metric	Label	F	D	G	B
v_x	F	-	$p_{adj} = 0.0019^{**}$	$p_{adj} = 0.2964$	$p_{adj} = 0.7985$
			$r = -0.4374$	$r = 0.2157$	$r = 0.1615$
			$\Delta = -31.12$	$\Delta = 16.31$	$\Delta = 9.78$
			CI = [-53.87, -8.37]	CI = [-6.23, 38.84]	CI = [-11.86, 31.41]
	D	-	-	$p_{adj} = 0.0000^{***}$	$p_{adj} = 0.0000^{***}$
				$r = 0.4727$	$r = 0.5153$
				$\Delta = 47.43$	$\Delta = 40.90$
				CI = [25.40, 69.45]	CI = [19.79, 62.01]
	G	-	-	-	$p_{adj} = 0.9581$
					$r = -0.1320$
					$\Delta = -6.53$
					CI = [-27.40, 14.35]
B	-	-	-	-	
				-	
				-	
				-	
Ω_{BL}	F	-	$p_{adj} = 0.0020^{**}$	$p_{adj} = 0.0001^{***}$	$p_{adj} = 0.0000^{***}$
			$r = -0.4804$	$r = -0.4476$	$r = -0.5425$
			$\Delta = -34.32$	$\Delta = -34.50$	$\Delta = -45.76$
			CI = [-55.95, -12.69]	CI = [-55.74, -13.25]	CI = [-67.20, -24.33]
	D	-	-	$p_{adj} = 1.0000$	$p_{adj} = 0.5758$
				$r = 0.0000$	$r = -0.1963$
				$\Delta = -0.18$	$\Delta = -11.45$
				CI = [-20.04, 19.68]	CI = [-31.50, 8.61]
	G	-	-	-	$p_{adj} = 0.5700$
					$r = -0.1550$
					$\Delta = -11.27$
					CI = [-30.91, 8.37]
B	-	-	-	-	
				-	
				-	
				-	
Ω_{DV}	F	-	$p_{adj} = 1.0000$	$p_{adj} = 0.0004^{***}$	$p_{adj} = 0.9979$
			$r = 0.0200$	$r = 0.4323$	$r = -0.0679$
			$\Delta = 1.71$	$\Delta = 32.37$	$\Delta = -3.83$
			CI = [-19.96, 23.38]	CI = [10.89, 53.86]	CI = [-25.50, 17.84]
	D	-	-	$p_{adj} = 0.0003^{***}$	$p_{adj} = 0.9772$
				$r = 0.4392$	$r = -0.0919$
				$\Delta = 30.67$	$\Delta = -5.54$
				CI = [10.81, 50.52]	CI = [-25.60, 14.52]
	G	-	-	-	$p_{adj} = 0.0000^{***}$
					$r = -0.4665$
					$\Delta = -36.21$
					CI = [-56.07, -16.35]
B	-	-	-	-	
				-	
				-	
				-	
Ω_V	F	-	$p_{adj} = 0.9337$	$p_{adj} = 0.0004^{***}$	$p_{adj} = 0.8646$
			$r = 0.0992$	$r = 0.4575$	$r = 0.1709$
			$\Delta = 7.19$	$\Delta = 32.07$	$\Delta = 8.09$
			CI = [-13.64, 28.01]	CI = [10.80, 53.34]	CI = [-11.75, 27.92]
	D	-	-	$p_{adj} = 0.0006^{***}$	$p_{adj} = 1.0000$
				$r = 0.4857$	$r = 0.0203$
				$\Delta = 24.88$	$\Delta = 0.90$
	G	-	-	-	$p_{adj} = 0.0003^{***}$
					$r = -0.5438$
B	-	-	-	$\Delta = -23.98$	
				CI = [-39.56, -8.41]	

	B	-	-	-	-
--	---	---	---	---	---